AIP | Applied Physics Letters

High repetition-rate neutron generation by several-mJ, 35 fs pulses interacting with free-flowing D2O

J. Hah, G. M. Petrov, J. A. Nees, Z.-H. He, M. D. Hammig, K. Krushelnick, and A. G. R. Thomas

Citation: Applied Physics Letters **109**, 144102 (2016); doi: 10.1063/1.4963819
View online: http://dx.doi.org/10.1063/1.4963819
View Table of Contents: http://scitation.aip.org/content/aip/journal/apl/109/14?ver=pdfcov
Published by the AIP Publishing

High repetition-rate neutron generation by several-mJ, 35 fs pulses interacting with free-flowing D_2O

J. Hah,[1] G. M. Petrov,[2] J. A. Nees,[1] Z.-H. He,[1,a)] M. D. Hammig,[3] K. Krushelnick,[1] and A. G. R. Thomas[1,4]
[1]*Center for Ultrafast Optical Science, University of Michigan, Ann Arbor, Michigan 48109, USA*
[2]*Naval Research Laboratory, Plasma Physics Division, 4555 Overlook Ave. SW, Washington, DC 20375, USA*
[3]*Department of Nuclear Engineering and Radiological Sciences, University of Michigan, Ann Arbor, Michigan 48109, USA*
[4]*Physics Department, Lancaster University, Bailrigg, Lancaster LA1 4YW, United Kingdom*

(Received 10 May 2016; accepted 19 September 2016; published online 4 October 2016)

Using several-mJ energy pulses from a high-repetition rate (1/2 kHz), ultrashort (35 fs) pulsed laser interacting with a ~10 μm diameter stream of free-flowing heavy water (D_2O), we demonstrate a 2.45 MeV neutron flux of 10^5/s. Operating at high intensity (of order 10^{19} W/cm^2), laser pulse energy is efficiently absorbed in the pre-plasma, generating energetic deuterons. These collide with deuterium nuclei in both the bulk target and the large volume of low density D_2O vapor surrounding the target to generate neutrons through $d(d,n)^3$He reactions. The neutron flux, as measured by a calibrated neutron bubble detector, increases as the laser pulse energy is increased from 6 mJ to 12 mJ. A quantitative comparison between the measured flux and the results derived from 2D-particle-in-cell simulations shows comparable neutron fluxes for laser characteristics similar to the experiment. The simulations reveal that there are two groups of deuterons. Forward moving deuterons generate deuterium–deuterium fusion reactions in the D_2O stream and act as a point source of neutrons, while backward moving deuterons propagate through the low-density D_2O vapor filled chamber and yield a volumetric source of neutrons. *Published by AIP Publishing.*
[http://dx.doi.org/10.1063/1.4963819]

Energetic neutrons have numerous applications in many fields, including medicine,[1] homeland security,[2] and material science.[3] Conventional fast neutron sources include deuterium–deuterium (D–D) and deuterium-tritium (D–T) fusion generators, as well as light-ion, photoneutron and spallation sources. Laser plasma interactions (LPI) in the relativistic regime can also generate charged particles and subsequently accelerate them to energies high enough to trigger nuclear fusion reactions resulting in neutron production.[4–16] Recent advances in ultra-high power laser technology now enable table-top scale systems, which may be further reduced in size for use as drivers for portable neutron generators in the future. One of the methods for neutron production is through the acceleration of high-energy ions (keV-MeV) impinging upon an appropriate converter target, such as deuterated plastic. Typically, thin solid targets are used in these experiments to accelerate deuterons.

Using solid targets in the form of a thin (1 μm) foil has some drawbacks for high repetition-rate (>kHz) operation; for example, one has to replace the target after each shot. To resolve target life-time issues, fast target replacement schemes have been introduced by some groups.[8,15,17–19] In particular, using ~100 mJ of pulse energy at 10 Hz repetition-rate, Ditmire *et al.*[8] used deuterium clusters, which were rapidly heated by the laser pulse (on a femtosecond time scale) and launched few keV deuterons to drive D–D nuclear fusion reactions.

In this letter, we report the production of neutrons using a high repetition rate femtosecond laser (1/2 kHz) at high intensities (>10^{19} W/cm^2 for vacuum focus) but low pulse energies (several-mJ) interacting with a heavy water stream. We demonstrate a conversion efficiency of laser energy into 2.45 MeV neutrons of ~10^{-8}, which is comparable to previous experiments that utilized table-top systems.[8,16,17,19–21]

Our experiment uses the Lambda-cubed (λ^3) laser facility at the University of Michigan. The λ^3 laser is a Ti:sapphire system ($\lambda = 800$ nm) producing laser pulses of duration $\tau = 35 \pm 2$ fs full-width-at-half-maximum (FWHM) with an amplified-spontaneous-emission (ASE) intensity contrast ratio of 10^8. However, for these experiments we deliberately introduce a pre-pulse split from the main pulse arriving 13 ns before the main pulse with an intensity contrast ratio of 10^3. This pre-pulse serves to generate a pre-plasma and increase the absorption of the main pulse energy.

The λ^3 laser operates at a 1/2 kHz repetition rate and delivers up to 18 mJ energy per pulse focused upon heavy water stream targets. The laser is focused to a 1.3 μm FWHM focal spot using an $f/1.4$ off-axis parabolic mirror, which produces a maximum peak intensity of 3×10^{19} W/cm^2 in vacuum. A commercial syringe pump (Teledyne Isco) is used to maintain a constant flow rate of heavy water through a 10 μm capillary, which produces a 15 μm diameter continuous flow of either heavy (D_2O) or light (H_2O) water, with a flow rate of 100 μl/min. The laser focus is set approximately 300 μm below the tip of the capillary and at the first surface normal to the flowing water. The chamber pressure is maintained at 20 Torr during the experiment by a roughing pump. Heavy water vapor originating from the stream fills the chamber and therefore acts as a catcher for accelerated deuterons for neutron generation. The experimental setup is shown in Fig. 1. Second harmonic light reflected from the

[a)]Now at Cymer, San Diego, CA, USA.

stream and off the parabolic mirror passes out of the chamber and is used to guarantee a normal incidence focus on the stream's surface. The CdTe x-ray detector is then used to minutely optimize this alignment to produce x-ray counts on every single shot. Fine target alignment is performed using piezo actuators (Newport Picomotor), for xyz-control of the paraboloid and the water stream.

In order to confirm the production of neutrons from D–D fusion reactions, we employ two different detection schemes. We use several bubble detectors (Bubble Tech Industries, BD-PND) located 4 cm from the interaction region at various angles with respect to the laser propagation direction, with the data shown in this Letter being taken at 45°. These bubble detectors contain superheated droplets (20 μm–50 μm in diameter), which vaporize into macroscopic bubbles (0.2 mm–0.5 mm in diameter) when they are irradiated by neutrons. In the energy range between 0.3 MeV and 10 MeV, the bubble detector has a flat response[22] and exhibits good linearity with respect to neutron dose.[23] Most importantly, these bubble detectors are insensitive to both x-rays and electron interactions. The bubble detector is also covered with a 1 mm thick aluminum tube to protect from direct laser irradiation.

Our bubble detector was independently calibrated for 2.45 MeV neutrons using a commercial neutron generator at the Neutron Science Laboratory at the University of Michigan (MP-320, Thermo Scientific). The 10^6 n/s neutron flux of the source yielded a calibration factor for the bubble detector of 6900 neutrons per bubble. Exposure of the bubble detector to the laser-based neutron source for 2 min accumulation periods resulted in the formation of up to 40 bubbles, corresponding to a calibrated neutron flux on the order of 10^5 n/s.

The second detection scheme consists of two plastic scintillators (ELJIN, EJ-204) coupled to photo-multiplier tubes (HAMAMATSU, H2431-50 biased at −2.5 kV). Using the plastic scintillators, neutron time-of-flight analysis is performed to determine the neutron energy spectrum. Two scintillators located at different distances and directions (2 m, 3.5 m, as in Fig. 1) measure the neutron time-of-flight signal. Two such recorded signals are shown in Fig. 2. Results from heavy water (black and red curves) are recorded at the stated distances and the light water signal (blue curves) is recorded independently at 3.5 m as a control. Note that the heavy water traces are the pulse shapes averaged over the 300 measurements that exceed the 2 mV noise floor in the neutron interval, and the light water trace is the pulse shape averaged over the 4000 measurements that exceed the 2 mV noise floor in the whole window.

All traces have x-ray peaks starting near 0 s, but only the two heavy water traces possess secondary peaks (black and red curves) corresponding to the relatively slow transit of the fusion neutrons to the detector following their creation. If D–D fusion occurs at the D_2O target, then the resulting 2.45 MeV neutron will interact with the scintillator 92 ns and 162 ns, for the 2 m and 3.5 m separations, respectively. However, the peaks for the 2 m and 3.5 m cases are observed at 110 ns and 182 ns, instead, showing that both signals are delayed by up to 20 ns from the expected arrival times. The effect of the delayed transit-time produces the down-shifted and broadened neutron energy spectra shown in the inset of Fig. 2. The delay is the result of neutron generation beyond the target as D^+ ions interact with D_2O vapor within the vacuum chamber, which will be detailed in the numerical simulation results shown below.

The D_2O stream will not have sharp boundaries predominantly because the main laser shot is preceded by a pre-pulse, which ablates the material and generates a pre-plasma

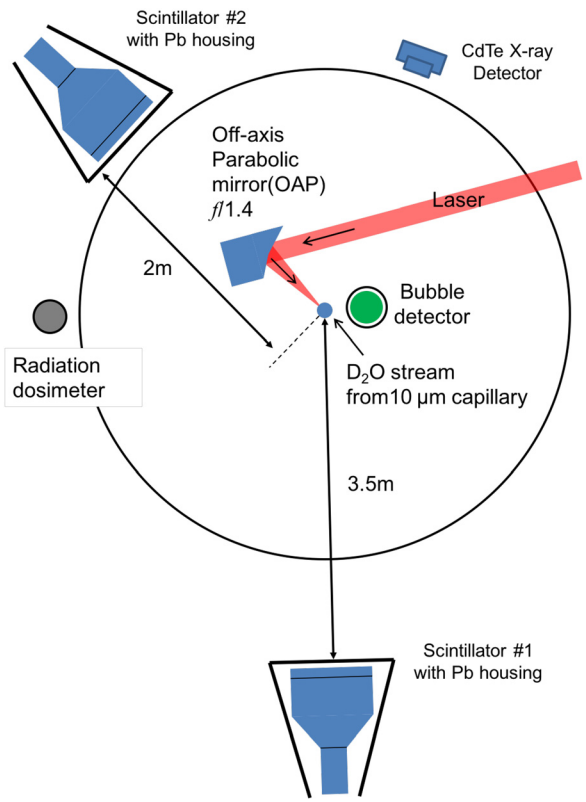

FIG. 1. Experimental setup. Note that scintillator distances are not to scale, the chamber diameter is 80 cm, and the chamber is filled with 20 Torr of heavy water vapor.

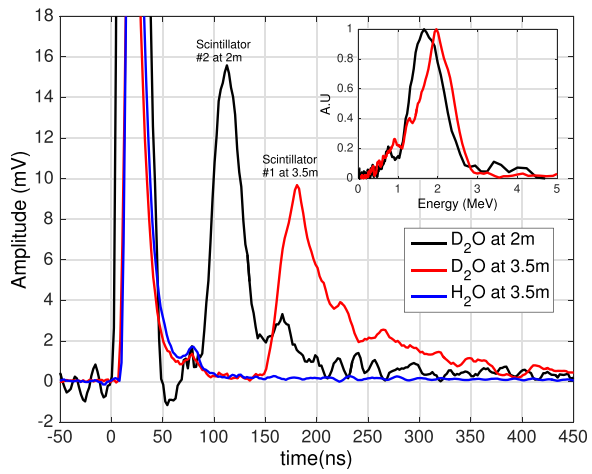

FIG. 2. Neutron time-of-flight analysis. The voltage signal derived from the photomultiplier tube following each x-ray interaction is averaged over 300 traces. The average trace derived from the light water target, shown in blue, is compared to the average traces derived from the heavy water target, when the neutron and x-ray sensitive scintillator is separated from the target by 2 m and 3.5 m, respectively. The inset shows the neutron energy spectrum derived from the approximate time-of-flight measurements.

surrounding the water target. The creation of this pre-plasma is beneficial as it increases the coupling efficiency of the laser energy to the production of hot electrons,[24–28] whose improvement enhances the energy of the deuterons. In Fig. 4, two data points (at 12 mJ and 13 mJ) are plotted for comparison, corresponding to no added large amplitude pre-pulse (but still the normal ASE and picosecond pre-pulses inherent to the laser). These points were taken under identical conditions to the points with a pre-pulse. Our results show that the introduced pre-pulse can generate more than an order of magnitude increase in neutron flux (n/s).

Numerical simulations are performed using a two-dimensional electromagnetic particle-in-cell code.[29,30] The D_2O target is approximated as a planar target at liquid density, having a pre-plasma with density exponentially decreasing away from the edge with a characteristic length of 1 μm at 1/*e*. This pre-plasma is estimated from measurements with a similar laser system interacting with water targets.[31] With an assumed focal spot size (D_{FWHM}) of 1 μm and a pulse duration (τ_{FWHM}) of 32 fs, the laser-water interaction is simulated for peak laser intensity variations between 1×10^{19} W/cm^2 and 3×10^{19} W/cm^2.

The on-target laser energy was varied between 3.7 and 11 mJ/shot. Particles are initialized with charge +1 for ions and −1 for electrons and during the simulations the ion charge of oxygen is dynamically incremented using a standard Monte Carlo scheme for collisional and optical field ionizations. At the beginning of the simulations, the number of particles per cell is 36 for deuterons and 18 for oxygen ions. The momentum distribution of deuterons is plotted in Fig. 3.

The phase-space plot reveals the dynamics of the interaction. First, the laser interacts primarily with the pre-plasma and all of the energetic ions originate from the pre-plasma region. The second intriguing observation is that there are two groups of deuterons: one group accelerated forward, and another group blown in the backward direction (towards the incoming laser direction). Their number is comparable; however, the backward moving deuterons are more energetic. In the forward direction the maximum normalized impulse is $p_x/(Mc) \sim 0.01$ and the corresponding momentum in the backward direction is doubled.

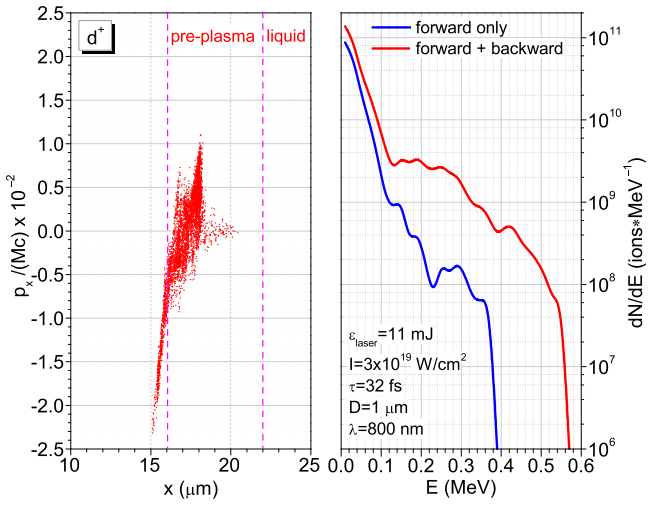

FIG. 3. (Left) Deuteron momentum $x - p_x$ phase space at the end of simulation, 192 fs. (Right) Deuteron energy spectrum.

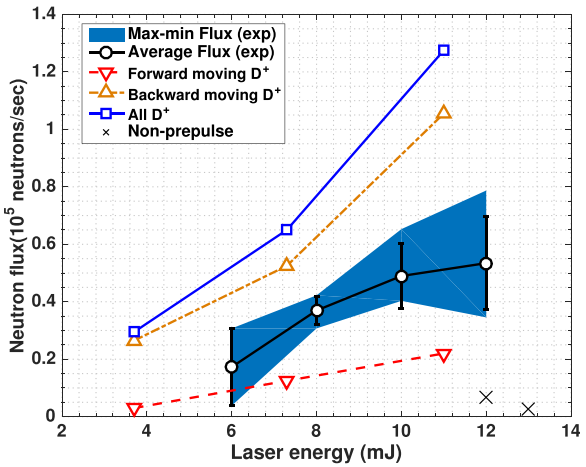

FIG. 4. Neutron flux as a function of energy from the experiments and simulations.

The particle-in-cell code is used to simulate only the laser plasma interaction, from which the deuteron spectrum was calculated. It is fitted with an exponential function (whose parameters are provided in the Table I). Deuterons with weights corresponding to this distribution are transported through the converter, and the neutron yield generated by these deuterons is calculated and accumulated. The angular distribution of neutrons is assumed to be isotropic, which is justified in the limit $E_d < 1$ MeV.[32]

The neutron production is very sensitive to the direction of the deuterons. The forward-directed deuterons find increasingly dense plasma, all the way up to liquid density in the stream. Since their range is only a few μm in water (7 μm for a 400 keV deuteron), the forward directed deuterons are stopped within the water stream.[33] These deuterons cause D–D fusion reactions and produce neutrons within the water stream. This is a *point source* of neutrons. In contrast, the backward directed deuterons move away from the main stream and interact with the gas/plasma with rapidly decreasing density, which transitions to the 20 Torr background density, where they have a much longer stopping distance. We estimated that at a background density in the chamber of 6.4×10^{17} cm^{-3}, a 400 keV deuteron has a stopping distance of 30 cm, similar to the chamber dimensions.

Therefore, the backward-moving deuterons will also contribute to neutron production *as a volumetric source*. This is illustrated in Fig. 4 which plots the neutron flux produced by forward and backward moving deuterons, as well as the sum of the two. The experimental data are also plotted for comparison. Table I provides more details such as the number of deuterons per shot, the neutron yield per deuteron and neutron yield per shot for forward and backward moving deuterons. The dominant neutron source is fusion from backward moving deuterons, and consequently, the larger fraction of neutrons has a volumetric origin. It has to be kept in mind, however, that we assumed complete stopping of the backward-directed deuterons; while in reality, some them may not be stopped by the low-density background gas. Thus, their contribution is likely overestimated. The volumetric nature of the neutrons was confirmed by the neutron time-of-flight measurements, which showed a delay and

TABLE I. Simulation result table.

Intensity (W/cm^2)	Energy (mJ)	# Deuterons > 10 keV	T (keV)	Neutron yield (n/ions)	Neutron yield (n/shot)	
1×10^{19}	3.7	1.4×10^9	18	4.0×10^{-9}	6	Forward
		3.3×10^9	45	18×10^{-9}	59	Total
2×10^{19}	7.3	2.6×10^9	30	9.5×10^{-9}	25	Forward
		5.0×10^9	55	26×10^{-9}	130	Total
3×10^{19}	11	3.7×10^9	35	12×10^{-9}	44	Forward
		6.7×10^9	65	38×10^{-9}	255	Total

increased width of the signal, which can only be interpreted as neutrons coming from different locations.

In conclusion, the production of D–D fusion neutrons is demonstrated with a millijoule level femtosecond laser system. Notably, the system operates at 1/2 kHz repetition rate, and requires neither the replacement of deuterated targets nor a catcher alignment. These features enable the generation of a neutron flux ($\sim 10^5$ n/s) which is comparable to other table-top laser based neutron sources, but for continuous all-day operation. Although the λ^3 system operates at 1/2 kHz, the present technology may enable operation at 10 kHz or higher, suggesting that such laser driven sources should be able to generate 10^6–10^7 n/s.

The authors would also like to thank Shaun Clarke and the University of Michigan Neutron Science Laboratory for use of the D–D generator. This material is based upon the work supported by the Air Force Office of Scientific Research Young Investigator Program under Award No. FA9550-12-1-0310, and partially supported by the Air Force Office of Scientific Research under Award No. FA9550-14-1-0282.

[1]V. Kononov, M. Bokhovko, O. Kononov, N. Soloviev, W. Chu, and D. Nigg, Nucl. Instrum. Methods Phys. Res. A **564**, 525 (2006).
[2]M. Roth, D. Jung, K. Falk, N. Guler, O. Deppert, M. Devlin, A. Favalli, J. Fernandez, D. Gautier, M. Geissel *et al.*, Phys. Rev. Lett. **110**, 044802 (2013).
[3]L. Perkins, B. Logan, M. Rosen, M. Perry, T. D. de la Rubia, N. Ghoniem, T. Ditmire, P. Springer, and S. Wilks, Nucl. Fusion **40**, 1 (2000).
[4]F. Floux, D. Cognard, L. G. Denoeud, G. Piar, D. Parisot, J. L. Bobin, F. Delobeau, and C. Fauquignon, Phys. Rev. A **1**, 821 (1970).
[5]T. Ditmire, J. W. G. Tisch, E. Springate, M. B. Mason, N. Hay, R. A. Smith, J. Marangos, and M. H. R. Hutchinson, Nature **386**, 54 (1997).
[6]G. Pretzler, A. Saemann, A. Pukhov, D. Rudolph, T. Schätz, U. Schramm, P. Thirolf, D. Habs, K. Eidmann, G. D. Tsakiris *et al.*, Phys. Rev. E **58**, 1165 (1998).
[7]P. A. Norreys, A. P. Fews, F. N. Beg, A. R. Bell, A. E. Dangor, P. Lee, M. B. Nelson, H. Schmidt, M. Tatarakis, and M. D. Cable, Plasma Phys. Controlled Fusion **40**, 175 (1998).
[8]T. Ditmire, J. Zweiback, V. Yanovsky, T. Cowan, G. Hays, and K. Wharton, Nature **398**, 489 (1999).
[9]L. Disdier, J. Garconnet, G. Malka, and J. Miquel, Phys. Rev. Lett. **82**, 1454 (1999).
[10]J. Zweiback, R. A. Smith, T. E. Cowan, G. Hays, K. B. Wharton, V. P. Yanovsky, and T. Ditmire, Phys. Rev. Lett. **84**, 2634 (2000).
[11]S. Karsch, S. Düsterer, H. Schwoerer, F. Ewald, D. Habs, M. Hegelich, G. Pretzler, A. Pukhov, K. Witte, and R. Sauerbrey, Phys. Rev. Lett. **91**, 015001 (2003).
[12]J. M. Yang, P. McKenna, K. W. D. Ledingham, T. McCanny, L. Robson, S. Shimizu, R. P. Singhal, M. S. Wei, K. Krushelnick, R. J. Clarke *et al.*, J. Appl. Phys. **96**, 6912 (2004).
[13]T. Žagar, J. Galy, J. Magill, and M. Kellett, New J. Phys. **7**, 253 (2005).
[14]L. Willingale, G. M. Petrov, A. Maksimchuk, J. Davis, R. R. Freeman, A. S. Joglekar, T. Matsuoka, C. D. Murphy, V. M. Ovchinnikov, A. G. R. Thomas *et al.*, Phys. Plasmas **18**, 083106 (2011).
[15]B. Hou, J. A. Nees, Z. He, G. Petrov, J. Davis, J. H. Easter, A. G. R. Thomas, and K. M. Krushelnick, Phys. Plasmas **18**, 040702 (2011).
[16]C. Zulick, F. Dollar, V. Chvykov, J. Davis, G. Kalinchenko, A. Maksimchuk, G. M. Petrov, A. Raymond, A. G. R. Thomas, L. Willingale *et al.*, Appl. Phys. Lett. **102**, 124101 (2013).
[17]S. Fritzler, Z. Najmudin, V. Malka, K. Krushelnick, C. Marle, B. Walton, M. S. Wei, R. J. Clarke, and A. E. Dangor, Phys. Rev. Lett. **89**, 165004 (2002).
[18]T. Nayuki, Y. Oishi, T. Fujii, K. Nemoto, T. Kayoiji, Y. Okano, Y. Hironaka, K. G. Nakamura, K.-i. Kondo, and K.-i. Ueda, Rev. Sci. Instrum. **74**, 3293 (2003).
[19]S. Ter-Avetisyan, M. Schnürer, D. Hilscher, U. Jahnke, S. Busch, P. V. Nickles, and W. Sandner, Phys. Plasmas **12**, 012702 (2005).
[20]G. Grillon, P. Balcou, J.-P. Chambaret, D. Hulin, J. Martino, S. Moustaizis, L. Notebaert, M. Pittman, T. Pussieux, A. Rousse *et al.*, Phys. Rev. Lett. **89**, 065005 (2002).
[21]K. W. Madison, P. K. Patel, D. Price, A. Edens, M. Allen, T. E. Cowan, J. Zweiback, and T. Ditmire, Phys. Plasmas **11**, 270 (2004).
[22]M. Gherendi, V. Kiptily, V. Zoita, S. Conroy, T. Edlington, D. Falie, A. Murari, A. Pantea, S. Popovichev, M. Santala *et al.*, J. Optoelectron. Adv. Mater. **10**, 2092 (2008).
[23]H. Ing, Radiat. Meas. **33**, 275 (2001).
[24]S. Bastiani, A. Rousse, J. P. Geindre, P. Audebert, C. Quoix, G. Hamoniaux, A. Antonetti, and J. C. Gauthier, Phys. Rev. E **56**, 7179 (1997).
[25]S. Lee, S. Kwon, K. Lee, Y.-H. Cha, D.-H. Kwon, S. Nam, K.-H. Yea, Y. W. Lee, Y. U. Jeong, Y. J. Rhee *et al.*, J. Korean Phys. Soc. **51**, 1695 (2007).
[26]P. McKenna, D. Carroll, O. Lundh, F. Nürnberg, K. Markey, S. Bandyopadhyay, D. Batani, R. Evans, R. Jafer, S. Kar *et al.*, Laser Part. Beams **26**, 591 (2008).
[27]T. Z. Esirkepov, J. K. Koga, A. Sunahara, T. Morita, M. Nishikino, K. Kageyama, H. Nagatomo, K. Nishihara, A. Sagisaka, H. Kotaki *et al.*, Nucl. Instrum. Methods Phys. Res. A **745**, 150 (2014).
[28]J. T. Morrison, E. A. Chowdhury, K. D. Frische, S. Feister, V. M. Ovchinnikov, J. A. Nees, C. Orban, R. R. Freeman, and W. M. Roquemore, Phys. Plasmas **22**, 043101 (2015).
[29]G. M. Petrov and J. Davis, Phys. Plasmas **18**, 073102 (2011).
[30]G. M. Petrov and J. Davis, Commun. Comput. Phys. **16**, 599 (2014).
[31]C. Orban, J. T. Morrison, E. A. Chowdhury, J. A. Nees, K. Frische, S. Feister, and W. M. Roquemore, Phys. Plasmas **22**, 023110 (2015).
[32]J. Davis, G. M. Petrov, T. Petrova, L. Willingale, A. Maksimchuk, and K. Krushelnick, Plasma Phys. Controlled Fusion **52**, 045015 (2010).
[33]J. F. Ziegler, M. Ziegler, and J. Biersack, Nucl. Instrum. Methods Phys. Res. B **268**, 1818 (2010).